sciendo

TATRA MOUNTAINS
Mathematical Publications

DOI: 10.2478/tmmp-2020-0007
Tatra Mt. Math. Publ. **75** (2020), 103–120

MACROPHAGE IMAGE SEGMENTATION BY THRESHOLDING AND SUBJECTIVE SURFACE METHOD

Seol Ah Park[1] — Tamara Sipka[2] — Zuzana Krivá[1] — Martin Ambroz[1] — Michal Kollár[1] — Balázs Kósa[1] — Mai Nguyen-Chi[2] — Georges Lutfalla[2] — Karol Mikula[1]

[1]Department of Mathematics and Descriptive Geometry, Slovak University of Technology in Bratislava, SLOVAKIA

[2]DIMNP, CNRS, Univ. Montpellier, Montpellier, FRANCE

ABSTRACT. We introduce two level-set method approaches to segmentation of 2D macrophage images. The first one is based on the Otsu thresholding and the second one on the information entropy thresholding, both followed by the classical subjective surface (SUBSURF) method. Results of both methods are compared with the semi-automatic Lagrangian method in which the segmentation curve evolves along the edge of the macrophage and it is controlled by an expert user. We present the comparison of all three methods with respect to the Hausdorff distance of resulting segmentation curves and we compare also their perimeter and enclosed area. We show that accuracy of the automatic SUBSURF method is comparable to the results of the semi-automatic Lagrangian segmentation.

1. Introduction

Macrophage is a type of motile white blood cell that plays a critical role in immune protection and homeostasis. However, chronic insults can subvert macrophage response, which becomes pathogenic and contributes to disease progression such as inflammatory diseases and cancer [6, 7, 13]. Macrophage changes its shape as it moves toward a wound. This shape change occurs as macrophages interact with surrounding cells and move between various tissue

2010 Mathematics Subject Classification: 68U10, 35K61, 65M08.
Keywords: image processing, segmentation, level-set methods, finite volume methods, thresholding, macrophages.
Supported by the Marie Skłodowska-Curie grant agreement no. 721537.

cells and extracellular matrix. While the image segmentation of macrophages can help to understand such interactions between macrophages and surrounding cells, it is also a challenging task due to their irregular shapes. In this paper, the cytoplasm of a macrophage in the transparent zebrafish is segmented from two-dimensional (2D) microscopy data. First, we use a 3 days old transgenic zebrafish larva (Tg(mpeg1:Gal4/UAS:Kaede)) in which green fluorescent protein Kaede is expressed under the control of macrophage-specific promoter mpeg1, so that macrophages produce the green fluorescent protein in their cytoplasm. After wounding of its caudal fin, migrating macrophages are imaged for 5 hours with a time step of 4 minutes and a z step of 4 μm using a Spinning disk Confocal microscope. Afterwards the three-dimensional (3D) images are projected onto a plane with the maximum intensity of 3D dataset overlap selected. The videos of the data are available on Zenodo (https://doi.org/10.5281/zenodo.3267228). We focus on the segmentation of a single macrophage in the resulting 2D image data, which is implemented by using two different approaches: automatic and semi-automatic (driven by an expert user).

The automatic approach is a combination of thresholding and the classical subjective surface segmentation (SUBSURF) method. The initial functions of the SUBSURF method are derived from two different thresholding techniques. The first one is the Otsu method [10], and the second one originates from the information entropy considering co-occurrence matrices [1,3]. Thresholds are automatically calculated for each image, and the images are simply modified into the foreground (above the threshold) and the background (under the threshold). These modified images are used for the initial condition of the SUBSURF method [11]. At the same time, the semi-automatic method based on the Lagrangian approach is used [9]. In this case, an initial point at the boundary of the macrophage is manually chosen, from which the segmentation curve evolves along the macrophage boundary. This process is repeated until the curve is closed and accurate segmentation is achieved. In this paper, this semi-automatic segmentation approach acts as a criterion for evaluating the performance of the automatic segmentation approach, because the former basically depends on expert judgement. We measure the Hausdorff distance between two curves from the semi-automatic and automatic methods to examine the accuracy of the curves matching [2]. Finally, the perimeter and area are calculated, allowing us to further evaluate the differences between the two approaches.

The paper is organized as follows. In section 2, we introduce two thresholding methods and the numerical discretization of the classical SUBSURF equation. Section 3 presents numerical results of the automatic segmentation and its comparison with the semi-automatic method. Lastly, we summarize and conclude briefly the results in section 4.

2. Mathematical Models and Numerical Methods

The classical SUBSURF method is a powerful segmentation method in such cases where an object has missing boundaries or contains background noise, such as the salt&pepper type [11]. However, it is known that quality of results depends on initial condition choice. Because the boundaries of most macrophages are complicated, it is expectable that the SUBSURF method would not work properly if the initial functions are arbitrary and do not consider at all the macrophage shape. On the other hand, the SUBSURF method can effectively complete missing parts of boundary, join adjacent level-lines, as well as rapidly remove a noise. To fully realize these benefits, it is important to set appropriate initial condition. In this work, macrophage images are binarized in order to get the initial condition for SUBSURF method by using two different thresholding methods: the Otsu method and the maximization of entropy-based functions.

2.1. Otsu thresholding

The Otsu method is a method to find a threshold that separates image into the object and the background in an automatic manner. The basic idea behind the Otsu method is to find the threshold such that the variability in each class (object, background) is as small as possible. It can be shown that this problem can be changed into maximizing between-class variance and can be solved very efficiently in a recursive fashion [10]. Therefore, if the histogram is bi-modal, the method can segment an object almost perfectly. In addition, the method is computationally cheap if only a single threshold is needed. The optimal threshold (k^*) from the Otsu method can be represented by

$$\sigma_B^2(k^*) = \max_{1 \le k < L} \sigma_B^2(k), \tag{1}$$

where σ_B denotes the variance between the foreground and background in the histogram, and L is the maximum intensity of the image. The Otsu thresholding method is able to properly distinguish several macrophage data when the intensity of the macrophage is quite clear compared to the background, even if it has either a thin or high-curvature structure. However, when the intensity inside the macrophage is comparable with the background noise, segmentation disconnects the object or loses parts of the macrophage since the Otsu method only considers the image intensity. Therefore, to more correctly segment such data, not only image intensity but also other factors have to be considered.

2.2. Entropy-based function with co-occurrence matrices

The image data we deal with in this paper represents a single macrophage. Therefore, it is reasonable that any dim part situated around bright parts can be considered as a part of the macrophage. In other words, adding spatial information can be helpful to calculate the threshold. This kind of approach has

previously been employed in several medical imaging studies [4, 12]. To add the spatial information of an image, a co-occurrence matrix is constructed [1], with which a certain intensity value maximizes the information entropy [3]. The maximum value of information entropy in terms of an image means that the image has the clearest bi-modal distribution of its histogram. Therefore, in principle, information entropy maximization is a similar approach to the Otsu method; however, the entropy method is more convenient when co-occurrence matrices are considered. The two required variables for the calculation of information entropy are the number of neighbours in the co-occurrence matrix and the image intensity. In [3], to get the spatial information just one pixel to the right and one pixel downward are explored, but in [12], q neighbours are inspected. The co-occurrence matrix, $T = \{t_{ij}\}$ for a $N \times N$ image can be described by

$$t_{ij} = \sum_{l=0}^{N} \sum_{k=0}^{N} \delta_q(l,k), \tag{2}$$

$$\delta_q(l,k) = 1 \begin{cases} f(l,k) = i, \quad f(l+q,k) = j, \\ \text{and/or} \\ f(l,k) = i, \quad f(l,k+q) = j, \end{cases} \quad \text{otherwise,} \quad \delta_q(l,k) = 0, \tag{3}$$

where q is changing from 1 to $N-1$ (number of inspected neighbours in our algorithm), i and j denote values of image intensity and $f(l,k)$ represents the gray level of the pixel at the spatial location (l,k).
With a particular threshold (t'), the co-occurrence matrix can be partitioned into four quadrants. The cell probabilities of each quadrant are calculated as

$$\begin{aligned} p_{ij}^{A}(q') &= \frac{t'_{ij}(q')}{\sum_{i=0}^{t'} \sum_{j=0}^{t'} t'_{ij}(q')}, \\ p_{ij}^{B}(q') &= \frac{t'_{ij}(q')}{\sum_{i=0}^{t'} \sum_{j=t'+1}^{L-1} t'_{ij}(q')}, \\ p_{ij}^{C}(q') &= \frac{t'_{ij}(q')}{\sum_{i=t'+1}^{L-1} \sum_{j=t'+1}^{L-1} t'_{ij}(q')}, \\ p_{ij}^{D}(q') &= \frac{t'_{ij}(q')}{\sum_{i=t'+1}^{L-1} \sum_{j=0}^{t'} t'_{ij}(q')}, \end{aligned} \tag{4}$$

where L is the maximum intensity of the image.

Here, $p_{ij}^{B}(q')$ and $p_{ij}^{D}(q')$ are used for the entropy-based function, which is the so-called joint entropy [3]:

$$H(q',t') = -\frac{1}{2}\left[\sum_{i=0}^{t'} \sum_{j=t'+1}^{L-1} p_{ij}^{B} \log p_{ij}^{B} + \sum_{i=t'+1}^{L-1} \sum_{j=0}^{t'} p_{ij}^{D} \log p_{ij}^{D}\right]. \tag{5}$$

For every t', the optimal number of neighbours (q^*) maximizing the joint entropy is calculated, and then the optimal threshold (t^*) maximizing $H_{joint}(q^*, t')$ is found.

2.3. Classical SUBSURF equation

2.3.1. Numerical Discretization

The classical SUBSURF method is described by

$$u_t = |\nabla u| \nabla \cdot \left(g \frac{\nabla u}{|\nabla u|} \right), \tag{6}$$

where u is the evolving level function. The function g is the so-called edge detector. We use

$$g(s) = \frac{1}{1 + K s^2}, \ K > 0, \tag{7}$$

where

$$s = |\nabla G_\sigma * I^0|, \quad I^0$$

being either original or thresholded image and G_σ is the Gaussian kernel, see also (13).

The time discretization of Eq. (6) is implemented with a semi-implicit scheme:

$$\frac{u^{n+1} - u^n}{\tau} = |\nabla u^n|_\epsilon \nabla \cdot \left(g \frac{\nabla u^{n+1}}{|\nabla u^n|_\epsilon} \right), \tag{8}$$

where τ is a uniform time step. Here, $|\nabla u^n|$ is regularized using the Evans--Sprucks approach as

$$|\nabla u^n|_\epsilon \approx \sqrt{(\nabla u^n)^2 + \epsilon^2},$$

where ϵ is a small arbitrary constant.

The space is discretized by a finite volume square grid with a volume (pixel) size h. For a pth pixel, the equation (6) is integrated, and by using Green's formula we get

$$\int_p \frac{1}{|\nabla u^n|_\epsilon} \frac{u^{n+1} - u^n}{\tau} \mathrm{d}\mathbf{x} = \int_{\partial p} g \frac{\nabla u^{n+1}}{|\nabla u^n|_\epsilon} \cdot \mathbf{n}_{pq} \mathrm{d}S, \tag{9}$$

where $\mathbf{n}_{pq}$ is the normal vector between the pth pixel and a neighbouring qth pixel.

Let us denote the center of the pth pixel as (i, j), where

$$i = 1, \ldots, N \quad \text{and} \quad j = 1, \ldots, N.$$

With the set of all neighbours (k, l), such that $k, l \in \{-1, 0, 1\}$, $|k| + |l| = 1$, the gradient of u on pixel edges can be represented by:

$$\begin{aligned} \nabla^{k0} u_{ij}^n &= \tfrac{1}{h}\left(u_{i+k,j}^n - u_{ij}^n, u_{ij}^{k,1} - u_{ij}^{k,-1}\right), \\ \nabla^{0l} u_{ij}^n &= \tfrac{1}{h}\left(u_{i,j+l}^n - u_{ij}^n, u_{ij}^{1,l} - u_{ij}^{-1,l}\right), \\ u_{ij}^{k,\pm 1} &= \tfrac{1}{4}\left(u_{ij}^n + u_{i,j\pm 1}^n + u_{i+k,j}^n + u_{i+k,j\pm 1}^n\right), \\ u_{ij}^{\pm 1,l} &= \tfrac{1}{4}\left(u_{ij}^n + u_{i\pm 1,j}^n + u_{i,j+l}^n + u_{i\pm 1,j+l}^n\right). \end{aligned} \tag{10}$$

Now we define

$$Q_{ij}^{kl;n} = \sqrt{\epsilon^2 + |\nabla^{kl} u_{ij}^n|^2},$$

$$\bar{Q}_{ij}^{kl;n} = \sqrt{\epsilon^2 + \frac{1}{4} \sum_{|k|+|l|=1} |\nabla^{kl} u_{ij}^n|^2}. \tag{11}$$

Therefore, the final discritized form of Eq. (6) is given by [8]

$$u_{ij}^{n+1} - u_{ij}^n = \frac{\tau}{h^2} \bar{Q}_{ij}^{kl;n} \sum_{|k|+|l|=1} g_{ij}^{kl,\sigma} \frac{u_{i+k,j+l}^{n+1} - u_{ij}^{n+1}}{Q_{ij}^{kl;n}}, \tag{12}$$

where h^2 is an area of pixel. Here, the edge detector function $g_{ij}^{kl,\sigma}$, is calculated by combining the gradients of the two types of pre-smoothed images, i.e., the original image (u_{ori}) and the binary image (u_{thr}) from each thresholding method, as

$$g_{ij}^{kl,\sigma} = \left(\frac{C_{ori}}{1 + K|\nabla u_{ori;\sigma}|^2} + \frac{C_{thr}}{1 + K|\nabla u_{thr;\sigma}|^2}\right), \tag{13}$$

where σ is the variance of the Gaussian filter. The C_{ori} and C_{thr} are coefficient of the edge detector for the original and binarized image, respectively.

3. Results

Segmentation is performed on a series of 75 images capturing a single macrophage. The solution of equation (12) is accompanied by the zero Dirichlet boundary condition, and the calculation is stopped when the following condition

is fulfilled:

$$\sum_{i=1}^{N}\sum_{j=1}^{N}|u_{ij}^{n+1}-u_{ij}^{n}|<\delta.$$

The final segmentation results were scaled into the interval [0,1] and the isoline 0.5 was selected as the boundary of macro-phage. The parameters used in the computations were

$$\begin{array}{lllllllll}\tau & = & 1, & & h & = & 1, & & K & = & 1000,\\ \sigma & = & 10^{-3}, & & \epsilon^2 & = & 10^{-10}, & & C_{ori} & = & 0.2,\end{array}$$

$$C_{thr}=0.8 \quad \text{and} \quad \delta=0.5.$$

Hereafter, the combination of the Otsu and classical SUBSURF methods is called the "O-SUBSURF" method, and likewise the SUBSURF method with co-occurrence matrices and information entropy is called the "E-SUBSURF" method.

3.1. Visual comparison of automatic and semi-automatic segmentation

In Figure 1–6, five images are selected. In the Figure 1, the left column shows the original images, and the middle and right columns show the binarized images resulting from the two thresholding methods. The Otsu thresholding method in the middle column well detects the macrophage when its intensity is (generally) uniformly distributed inside the macrophage and distinguishable from the background noise [(2)-O, (3)-O]. In most cases, this phenomenon appears when the macrophage squeezes itself. On the other hand, parts of the macrophage tend to have weak intensity when it stretches itself, in which case Otsu thresholding cannot well resolve the structure ((1)-O, (4)-O). On the other hand, as it is seen in the right column of the figure, the co-occurrence matrices with information entropy maximization can well detect such dim parts of the images ((1)-E, (4)-E) because the thresholds are lower than those of the Otsu method. The reason is that when the structures are close to each other, the weights of the structures in the co-occurrence matrix are increased, regardless of if it is background noise or the macrophage. Because of this feature, the macrophage is detected to be thicker than those of the Otsu method, and also the background noise can be easily captured ((1)-E, (2)-E, (4)-E). The Figure 2–6 show segmentation results obtained using different methods. The top-left panels of Figure 2--6 (yellow lines) denote segmentation results by the semi-automatic method. The top-right and bottom-left represent segmented boundaries from O-SUBSURF and E-SUBSURF methods and are denoted by blue and green lines, respectively. If the captured background noise occupies a small portion, it is rapidly removed by the SUBSURF method without losing macrophage shape because the small noise has a large curvature, as it is seen in Figure 1 (4)-E and in Figure 5.

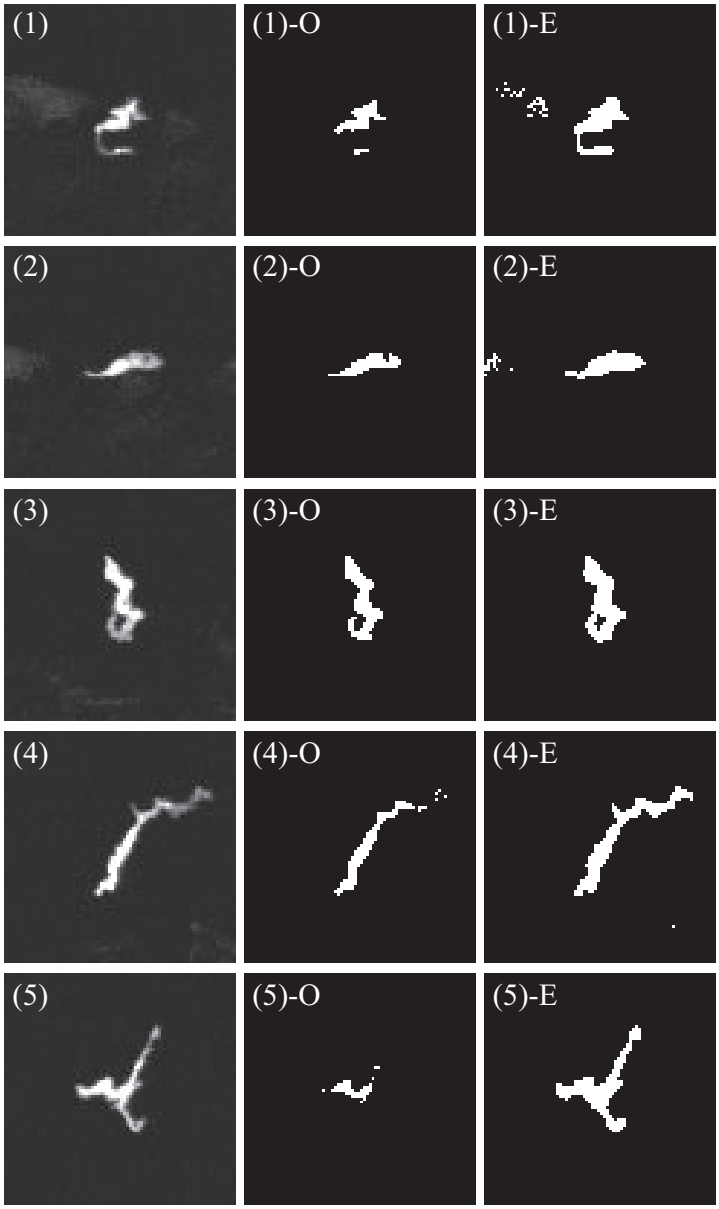

FIGURE 1. Five different time moments of image series. The first column shows the original macrophage images, and the second and third columns show binarized images from Otsu thresholding ((#)-O) and entropy thresholding ((#)-E), respectively.

TABLE 1. Differences of perimeters (ΔP) and areas (ΔA) between the semi-automatic and automatic methods for u_c.

Time	ΔP	ΔA	**Time**	ΔP	ΔA	**Time**	ΔP	ΔA	**Time**	ΔP	ΔA
0	1.20	32.93	18	2.68	18.45	36	10.38	39.56	54	10.39	27.74
1	1.13	16.10	19	0.56	13.63	37	5.64	29.90	55	10.91	32.07
2	5.77	23.78	20	4.89	23.41	38	0.45	32.25	56	11.32	11.77
3	0.41	16.06	21	2.87	16.62	39	5.82	43.61	57	5.39	12.25
4	4.03	21.14	22	1.39	30.09	40	11.10	34.83	58	0.27	32.57
5	6.18	26.43	23	0.68	23.95	41	3.57	30.28	59	16.07	13.48
6	13.37	11.82	24	5.41	33.99	42	7.28	44.54	60	14.48	27.59
7	18.30	0.27	25	3.93	9.45	43	2.08	14.76	61	7.07	8.39
8	0.21	7.63	26	22.15	8.30	44	2.83	23.80	62	14.06	3.07
9	0.36	15.14	27	16.51	14.65	45	6.17	3.03	63	0.04	26.50
10	1.50	23.89	28	14.46	11.86	46	4.54	9.65	64	9.50	7.34
11	0.37	10.40	29	2.33	0.56	47	4.26	24.17	65	9.56	30.17
12	0.61	9.39	30	21.50	8.44	48	5.54	16.92	66	4.51	26.66
13	4.25	17.29	31	1.06	26.38	49	21.36	1.67	67	8.80	5.42
14	2.69	21.37	32	5.38	7.30	50	4.79	3.89	68	2.04	49.64
15	0.06	21.27	33	1.22	3.47	51	10.50	11.20	69	10.17	54.62
16	2.02	25.74	34	7.79	1.92	52	0.73	33.09	70	4.36	35.03
17	3.94	27.44	35	8.47	9.19	53	5.18	11.91	71	7.85	28.80
									72	3.64	43.53
									73	4.86	9.36
									74	9.48	24.79
									AVG	6.22	20.13
									SD	5.46	12.38

However, if the noise intensity is comparable with the macrophage one, SUBSURF cannot easily get rid of the noise, as in Figure 2 (1)-E. Comparison indicates that the segmentation shapes given by the O-SUBSURF method tend to be more narrow (blue lines) while those of the E-SUBSURF method tend to be more broad (green lines) than the results from the semi-automatic method. To utilize the benefits and improve the drawbacks of the two automatic methods, we combine the final solutions with certain weight factors.

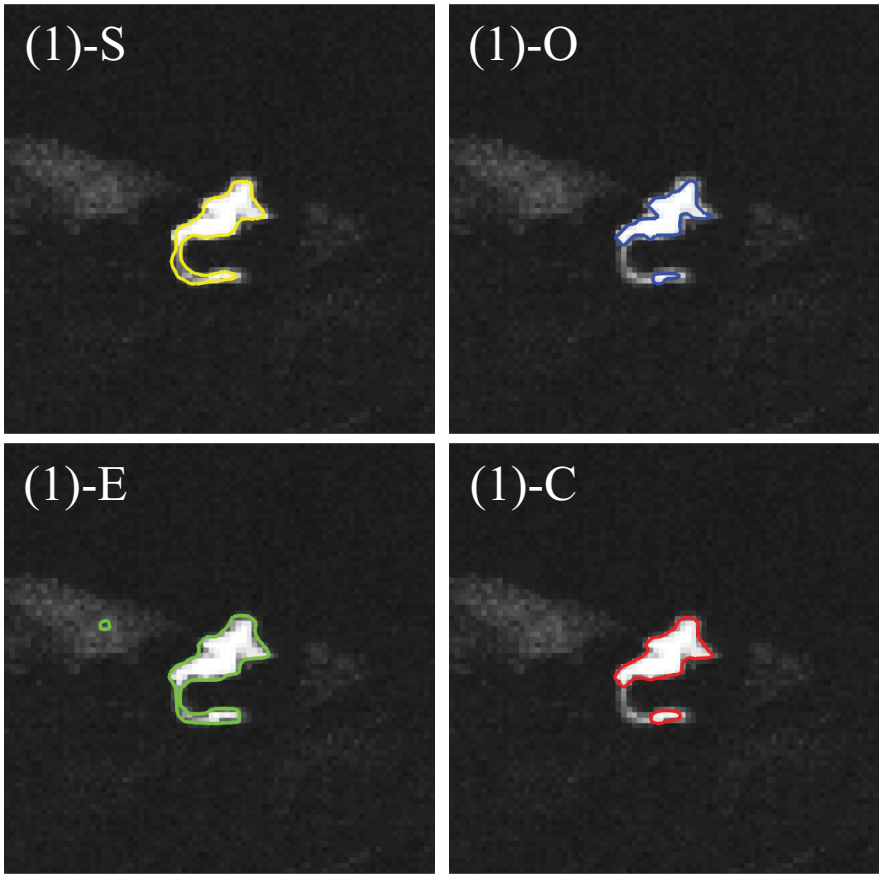

FIGURE 2. The 7th image in whole sequence: Segmentation results from the thresholding methods (the first row of Figure 1) and SUBSURF method. The yellow lines come from the semi-automatic segmentation results ($(1)-S$). The blue and green lines are the final results from the O-SUBSURF ((1)-O) and E-SUBSURF methods ((1)-E), respectively. In the bottom-right panel, the red lines describe u_c, combination of both methods ((1)-C). The coloured version of the article can be found on the journal web-site, `http://tatra.mat.savba.sk(publishedvolume)`.

By setting the solution from O-SUBSURF as u_O and that from E-SUBSURF as u_E, then both solutions are combined and level line of 0.5 is selected. The combined solution (u_c) is described as $u_c = \omega_O u_O + \omega_E u_E$. In this implementation, $\omega_O = 0.4$ and $\omega_E = 0.6$ were used; results are presented as red lines in Figure 2–6. Although u_c fails to detect the dim parts in the bottom-right panel of Figure 2, the rest of the results are very close to those from the semi-automatic method.

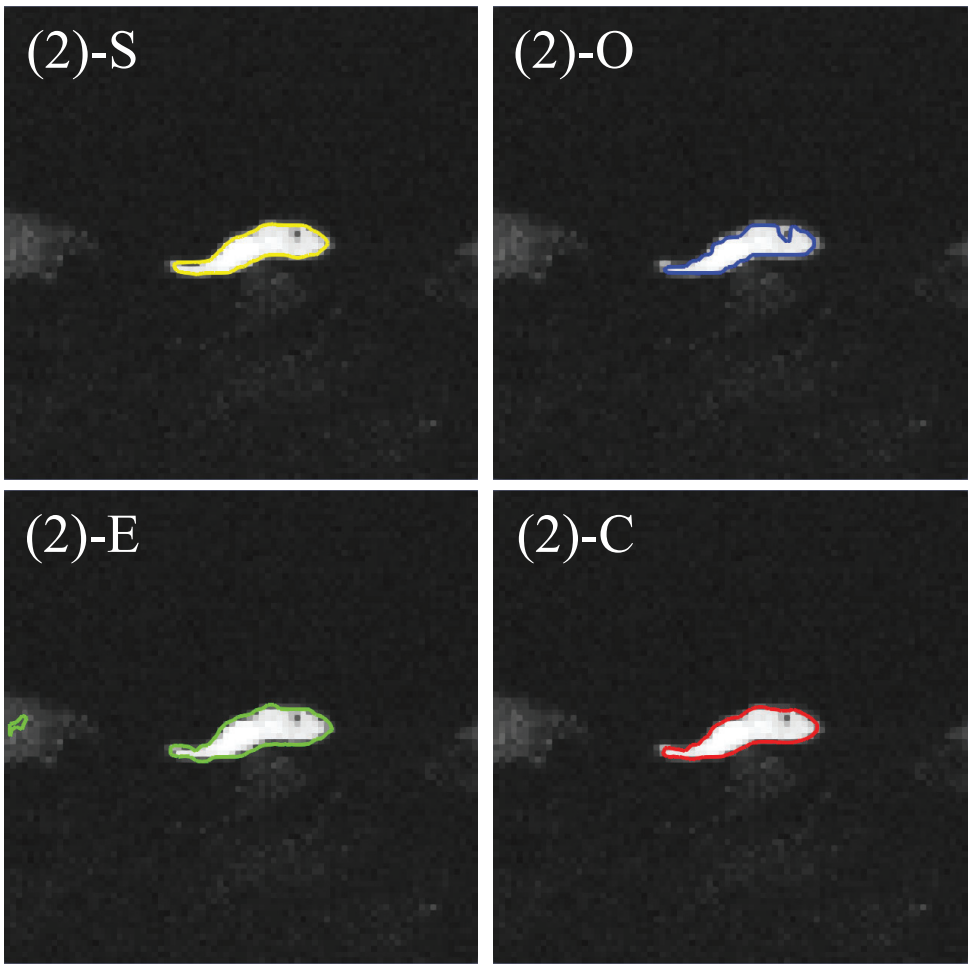

FIGURE 3. The 8th image in whole sequence: Segmentation results from the thresholding methods (the second row of Figure 1) and SUBSURF method. The yellow lines come from the semi-automatic segmentation results $((2) - S)$. The blue and green lines are the final results from the O-SUBSURF ((2)-O) and E-SUBSURF methods ((2)-E), respectively. In the bottom-right panel, the red lines describe u_c, combination of both methods ((2)-C). The coloured version of the article can be found on the journal web-site, `http://tatra.mat.savba.sk(publishedvolume).`

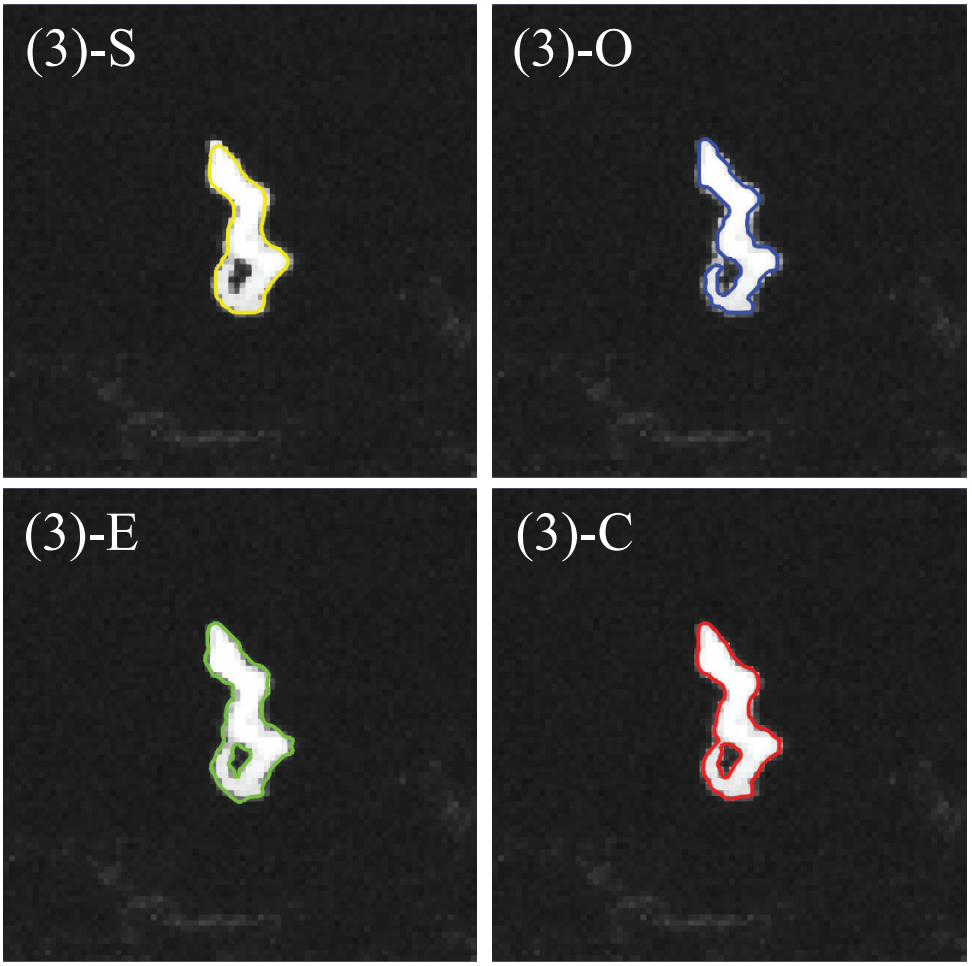

FIGURE 4. The 49th image in whole sequence: Segmentation results from the thresholding methods (the third row of Figure 1) and SUBSURF method. The yellow lines come from the semi-automatic segmentation results ($(3)-S$). The blue and green lines are the final results from the O-SUBSURF ((3)-O) and E-SUBSURF methods ((3)-E), respectively. In the bottom-right panel, the red lines describe u_c, combination of both methods ((3)-C). The coloured version of the article can be found on the journal web-site, `http://tatra.mat.savba.sk(publishedvolume).`

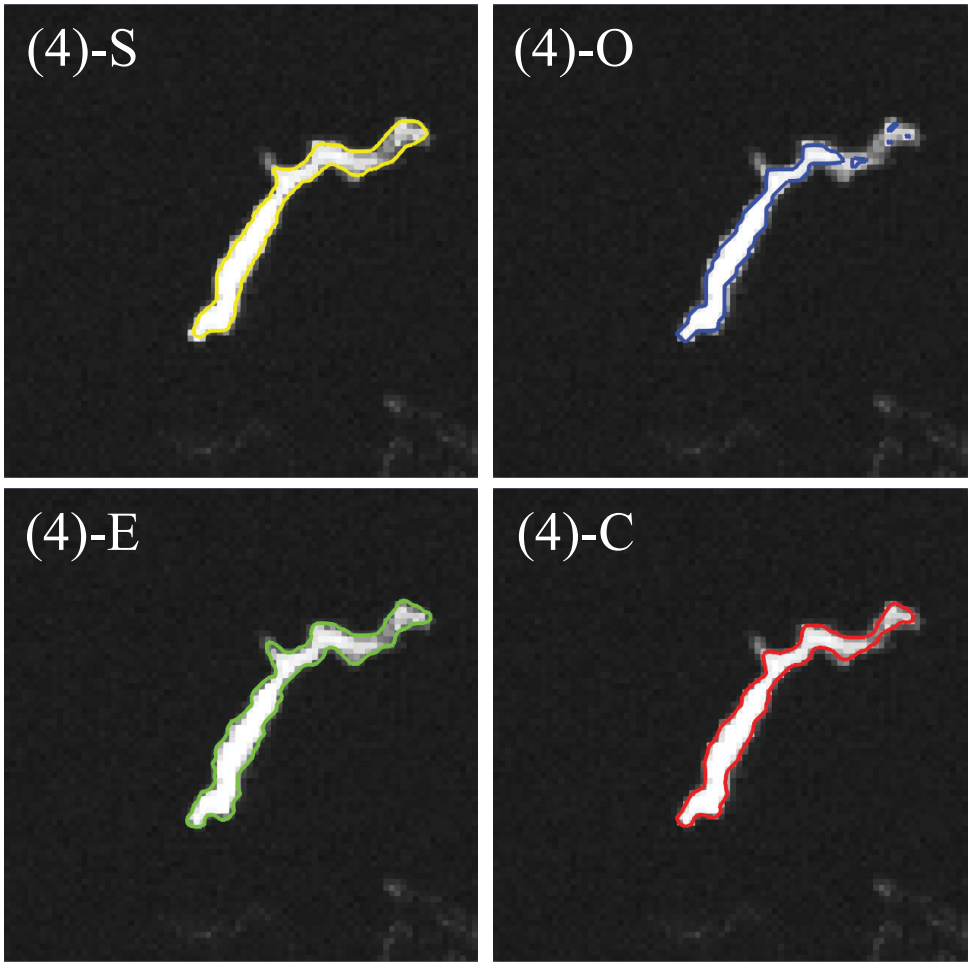

FIGURE 5. The 67th image in whole sequence: Segmentation results from the thresholding methods (the fourth row of Figure 1) and SUBSURF method. The yellow lines come from the semi-automatic segmentation results ((4)-S). The blue and green lines are the final results from the O-SUBSURF ((4)-O) and E-SUBSURF methods ((4)-E), respectively. In the bottom-right panel, the red lines describe u_c, combination of both methods ((4)-C). The coloured version of the article can be found on the journal web-site, `http://tatra.mat.savba.sk(publishedvolume)`.

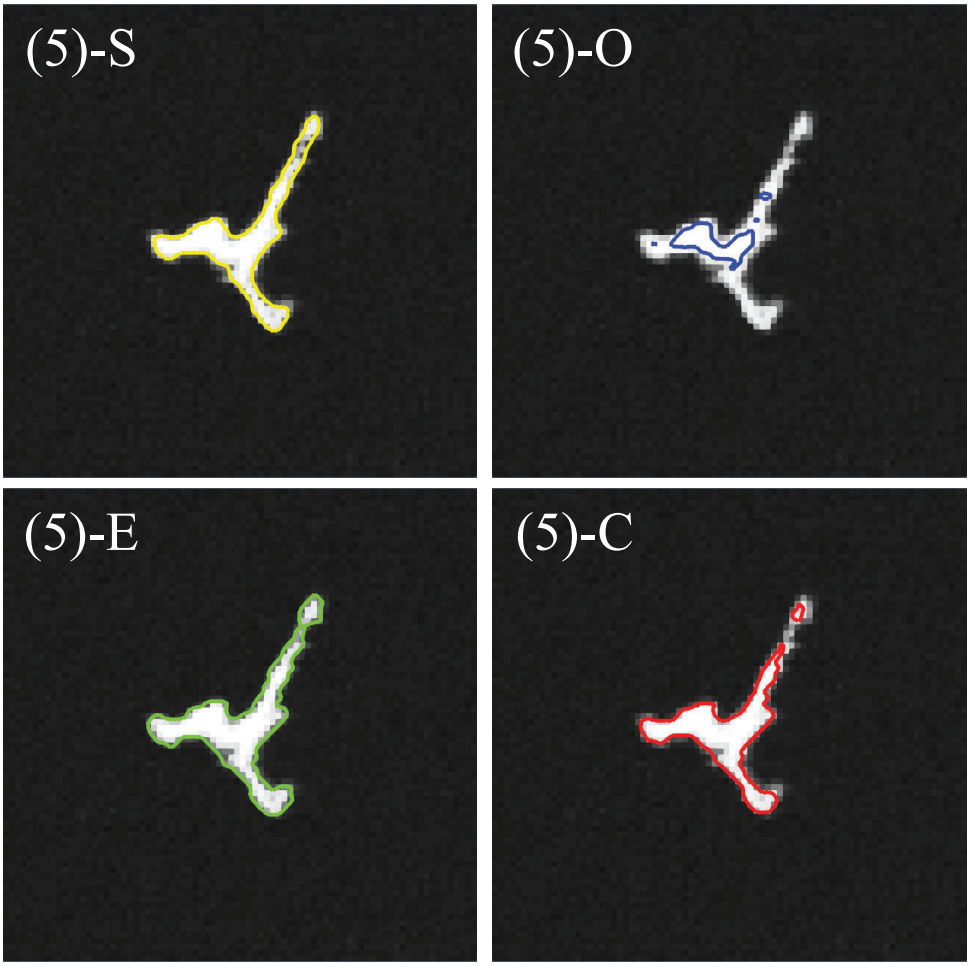

FIGURE 6. The 35th image in whole sequence: Segmentation results from the thresholding methods ((the fifth row of Figure 1)) and SUBSURF method. The yellow lines come from the semi-automatic segmentation results ((5)-S). The blue and green lines are the final results from the O-SUBSURF ((5)-O) and E-SUBSURF methods ((5)-E), respectively. In the bottom-right panel, the red lines describe u_c, combination of both methods ((5)-C). The coloured version of the article can be found on the journal web-site, `http://tatra.mat.savba.sk(publishedvolume).`

3.2. Quantitative comparison between automatic and semi-automatic segmentation

In this section, the automatic segmentation results are compared to those from the semi-automatic method using the Hausdorff distance [5] and the perimeter and area of the macrophage. The perimeters are calculated by summing all the distances between two adjacent points of the isoline, and the areas are calculated via Gauss's area formula. If the boundary from the automatic method has more than a single isoline, the calculations are implemented independently to each closed isoline and summed from all outcomes. In the real scale, the pixel size on the images is corresponding to 0.326 μm. Therefore, the unit of the calculated results in Figure 7, Figure 8 and Table 1 is 0.326 μm. Figure 7 shows the Hausdorff distances. As it is seen in Figure 7, several values of the Hausdorff distance in the results from the E-SUBSURF method are high. The reason is that those final results contain boundaries of the background noise, and the noise is relatively far from the macrophages. Whereas, in case of the O-SUBSURF method, the large values of the Hausdorff distance are due to missing parts of the macrophages. For example, the largest Hausdorff distance from the O-SUBSURF method is 35^{th} image (the bottom images in Figure 1 and Figure 6), and its perimeter and area also show the biggest difference from those of the semi-automatic method. Contrarily, data with big Hausdorff distances in the E-SUBSURF method do not show striking differences from the perimeter and area of the semi-automatic method (Figure 8). To indicate how big the Hausdorff distances are in terms of macrophage size, the ratio of the Hausdorff distances and the perimeters is measured. The median of d_H/d_P from the O-SUBSURF, E-SUBSURF methods and combined solution are approximately 0.032, 0.02 and 0.022, respectively. This indicates that mismatching O-SUBSURF, E-SUBSURF and combined methods from the semi-automatic segmentation i s roughly represented by 3.2 %, 2 % and 2.2 %, respectively. As shown in Figure 8, most areas from O-SUBSURF are smaller than the semi-automatic results, whereas most areas from E-SUBSURF are larger than the semi-automatic method because of the co-occurrence matrices. The combined result, u_c, not only has small values of Hausdorff distances but is also relatively similar to the perimeters and areas of the semi-automatic method (red lines in Figure 7 and 8). In the results of the combined level-lines, there is no more captured background noise and no substantial missing parts; however, there are still small missing parts and a hole inside the macrophage (Figure 4). Because the split part from the Otsu method (top-right panel in Figure 4) has similar intensity with neighbours, the semi-automatic method evolves the curve by covering this part. In the contrast to the semi-automatic method result, all results from automatic methods distinguish the hole inside the macrophage. Therefore, the hole from the automatic method leads to a big difference in the Hausdorff distance. To figure out which result is correct, it may need to discuss it from a biological point of view.

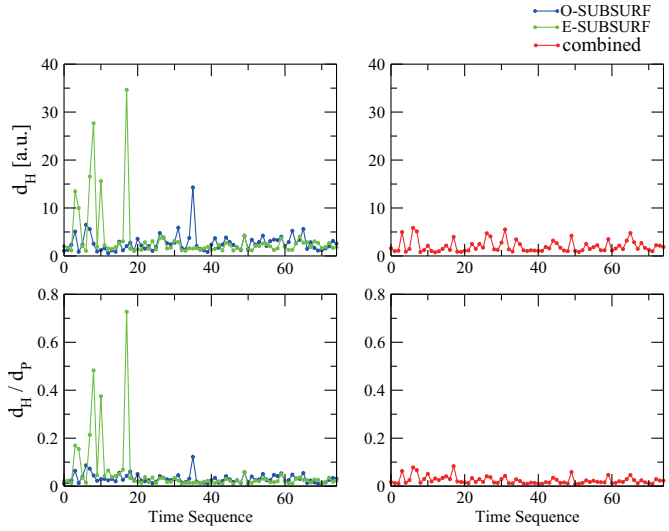

FIGURE 7. The Hausdorff distances (d_H) and the ratio (d_H/d_P) of those distances to the perimeters for the semi-automatic method. O-SUBSURF, E-SUBSURF, and combined are from u_O, u_E, and u_c, respectively.

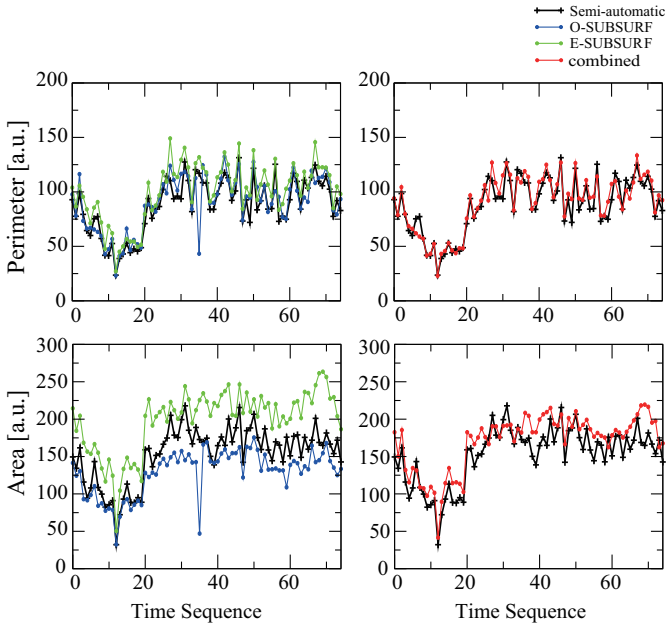

FIGURE 8. Perimeters and areas from four different cases. The Black lines with cross symbol results by semi-automatic method. O-SUBSURF, E-SUBSURF, and combined are from u_O, u_E, and u_c, respectively.

Quantitative perimeter and area difference information for all data is presented in Table 1. In this calculation, ΔP and ΔA are the absolute deviations of the perimeter and area, respectively. **AVG** and **SD** are average and standard deviation of ΔP and ΔA, defined as:

$$\mathbf{AVG} = \frac{1}{75}\sum_{i=0}^{i=74}\Delta x_i, \qquad \mathbf{SD} = \sqrt{\frac{1}{75}\sum_{i=0}^{i=74}(\Delta x_i - \mathbf{AVG}(x))^2},$$

where x is either perimeter or area, i denotes image sequence and 75 is the total number of images. Since **AVG** in Table 1 is the standard deviation of the differences between semi-automatic and automatic methods, **AVG** can be considered as an error for automatic segmentation. Hence, the errors of proposed auto-segmentation method can be represented as 6.22 ± 5.46 and 20.13 ± 12.38 for the perimeter and area, respectively.

4. Conclusion

The segmentation of a single macrophage from 2D data was achieved via automatic and semi-automatic methods. In the former, two types of thresholding techniques were carried out and used as the initial functions of the classical SUBSURF method, while in the latter, the Lagrangian method was utilized as the gold standard for examining the automatic segmentation method. The final segmentation functions from the classical SUBSURF method were scaled into interval $[0, 1]$ with the selected middle value. The performance of automatic segmentation was measured with the Hausdorff distances in a view of matching the boundary shapes with those from the semi-automatic method. In addition, geometric information (perimeter, area) and its difference between the two methods was calculated. Based on these measurements, the combination of the level-lines from O-SUBSURF and E-SUBSURF gave reasonable results when compared to the semi-automatic segmentation.

REFERENCES

[1] AHUJA, N.—ROSENFELD, A.: *A Note on the Use of Second-Order Gray Level Statistics for Threshold Selection*, IEEE Transactions on Systems, Man, and Cybernetics **8**(12) (1978), 895-898.

[2] ALT, H.—BEHRENDS, B.—BLÖMER, J.: *Approximate matching of polygonal shapes*, Annals of Mathematics and Artificial Intelligence **13**(3-4) (1995), 251–265.

[3] CHANG, C. I.—CHEN, K.—WANG, J.—ALTHOUSE, M. L.: *A relative entropy-based approach to image thresholding*, Pattern Recognition **27**(9) (1994), 1275–1289.

[4] CHANWIMALUANG, T.—FAN, G.: *An efficient blood vessel detection algorithm for retinal images using local entropy thresholding.* In:*Proceedings of the 2003 International Symposium on Circuits and Systems, May, 2003.* IEEE Vol. 5, 2003, pp. 21–24.

[5] HUTTENLOCHER, D. P.—KLANDERMAN, G. A.—RUCKLIDGE, W. A.: *Comparing Images Using the Hausdorff Distance*, IEEE Transactions on Pattern Analysis and Machine Intelligence **15**(9) (1993), 850–863.

[6] LEWIS, C. E.—POLLARD, J. W.: *Distinct role of macrophages in different tumor microenvironments*, Cancer Research **66** (2006), no. 2, 605–612.

[7] MANTOVANI, A.—SOZZANI, S.—LOCATI, M.—ALLAVENA, P.—SICA, A.: *Macrophage polarization: tumor-associated macrophages as a paradigm for polarized M2 mononuclear phagocytes*, Trends in Immunology **23** (2002), no. 11, 549–555.

[8] MIKULA, K.—PEYRIÉRAS, N.—REMEŠIKOVÁ, M.—SARTI, A.: *3 D embryogenesis image segmentation by the generalized subjective surface method using the finite volume technique*, Finite Volumes for Complex Applications V: Problems and Perspectives (2008), 585–592.

[9] MIKULA, K.—URBÁN, J.—KOLLAR, M.—AMBROZ, M.—JAROLIMEK, I.—SIBIK J.—SIBIKOVA, M.: *Semi-automatic segmentation of NATURA 2000 habitats in Sentinel--2 satellite images by evolving open curves*, Discrete and Continuous Dynamical Systems--series S, (submitted).

[10] OTSU, N.: *A threshold selection method from gray-level histograms*, IEEE transactions on systems, man, and cybernetics **9** (1979), no. 1, 62–66.

[11] SARTI, A.—MALLADI, R.—SETHIAN, J. A.: *Subjective surfaces: A method for completing missing boundaries*, Proceedings of the National Academy of Sciences **97** (2000), no. 12, 6258–6263.

[12] WU, C. M.—CHEN, Y. C.—HSIEH, K. S.: *Texture features for classification of ultrasonic liver images*, IEEE Transactions on medical imaging **11** (2) (1992), 141–152.

[13] WYNN, T. A.—CHAWLA, A.—POLLARD, J. W.: *Macrophage biology in development, homeostasis and disease*, Nature **496** (2013), no. 7446, 445–455.

Received July 4, 2019

[1] *Department of Mathematics and Descriptive Geometry*
Slovak University of Technology in Bratislava
Radlinského 11
810 05 Bratislava
SLOVAKIA

E-mail: standup1014@gmail.com
zuzkakriva13@gmail.com
ambroz.martin.ml@gmail.com
michalkollar27@gmail.com
kosabalu@gmail.com
karol.mikula@gmail.com

[2] *DIMNP, CNRS,*
University Montpellier
Place E.Bataillon-Building 24, 2nd floor
34095 Montpellier Cedex 05
FRANCE

E-mail: tamara.sipka@etu.umontpellier.fr
mai-eva.nguyen-chi@umontpellier.fr
georges.lutfalla@umontpellier.fr